Available online at www.sciencedirect.com
SCIENCE DIRECT
Journal of Catalysis 231 (2005) 151–158
JOURNAL OF CATALYSIS
www.elsevier.com/locate/jcat

Nanoparticles of gold on γ-Al_2O_3 produced by dc magnetron sputtering

Gabriel M. Veith *, Andrew R. Lupini, Stephen J. Pennycook, Gary W. Ownby, Nancy J. Dudney

Condensed Matter Sciences Division, Oak Ridge National Laboratory, Oak Ridge TN 37831, USA

Received 14 October 2004; revised 3 December 2004; accepted 6 December 2004

Abstract

This paper describes a one-step magnetron sputtering technique for the preparation of supported catalyst particles that has a number of advantages over existing methods. In order to demonstrate the effectiveness of this technique, a supported gold on γ-Al_2O_3 oxidation catalyst has been prepared. This catalyst is as active as catalysts prepared via traditional chemical methods for the oxidation of carbon monoxide (TOF 1.1 conversions/surface Au atom/second at 300 K and 16% CO/8% O_2/He). Aberration-corrected scanning transmission electron microscopy demonstrates that this technique produces gold nanoparticles in a size range that is claimed in the literature to be most active (about 2 nm).

Keywords: Sputtering; Oxidation catalysts; XPS; Aberration-corrected STEM; Gold nanoparticles; CO oxidation; γ-Al_2O_3

1. Introduction

The discovery of catalytic activity from gold nanoparticles for the oxidation of carbon monoxide in 1989 by Haruta et al. [1] led to a great deal of research directed at exploring and understanding the unique properties of a material previously thought to be chemically inert. As a result there is a growing body of scientific literature detailing the synthesis and reactivity of Au nanoparticles in a variety of reactions. However, as Wolf and Schüth pointed out in 2002, "the reproducibility of highly active gold catalysts is typically very low" [2]. This lack of reproducibility is due to the large number of synthetic preparation methods and the subsequent treatments of the catalysts (i.e., annealing, aging), which subtly affect the catalytic properties [2]. In addition, most of these techniques are not industrially feasible because of the large amount of water required or the prohibitive cost of reagents.

There are two different classes of techniques for making gold nanoparticles: chemical and physical. Chemical methods typically involve the decomposition or precipitation of gold from a gold precursor like $HAuCl_4$. These are the most widely used techniques because of the availability of reactants and the low costs on the laboratory scale. These chemical methods are described in several reviews [3–8].

Physical methods typically involve the production of gas-phase gold atoms or clusters. One of the simplest methods for producing gas-phase gold atoms is to thermally evaporate gold under high vacuum followed by the deposition of the Au on a single-crystal substrate [9,10]. Chemical vapor deposition (CVD) also has been used to prepare gold catalysts [11,12]. CVD techniques rely on the decomposition of a gold precursor, such as dimethyl gold β-ketone, to coat a substrate [11,12]. Recently Arrii et al. reported the synthesis of gold nanoparticles on a variety of supports by laser vaporization of a gold target [13].

Our preparation method can briefly be described as the sputtering of a high-purity gold target with argon ions, followed by the subsequent deposition of the sputtered gold atoms on the surface of a moving powder support material to create a uniform dispersion of nanoparticles. The general principle was described in 1979 [14], and the first results were reported in 1983 by Takeuchi and Wise, who used radio-frequency (RF) sputtering to prepare Pt particles (< 30 Å diameter) on χ-Al_2O_3 [15]. In 1989 Albers et al. reported the synthesis of 22–29 Å Pt particles via direct current sputtering of Pt foil [16]. In 1997 Wang et al. reported using

* Corresponding author.
E-mail address: veithgm@ornl.gov (G.M. Veith).

0021-9517/$ – see front matter
doi:10.1016/j.jcat.2004.12.008

a similar technique to coat SiC powders with Cu metal with the intent of improving interface properties [17]. During the course of this work, Ensinger and Müller reported coating tumbling Al_2O_3 and WC powders with the use of a beam of noble gas ions to sputter a Au or Pt target [18]. RF sputtering has previously been reported to be a good technique for making small particles of gold on a thin film surface [19].

This report details the use of magnetron sputtering to create nanoparticles of gold on a high-surface-area powder support along with the subsequent characterization of the gold particles by aberration corrected electron microscopy. Our results show that the gold catalysts prepared by this method are as active as conventionally prepared CO oxidation catalysts. This technique has several advantages over existing preparation methods. For example, there is no contamination from solvent or precursor molecules on the surface, and no heating is required to decompose the precursors. The process is economical and environmentally friendly, since the excess gold is recoverable from the chamber and there is no liquid waste. Finally, it is also adaptable to a wide range of catalyst materials and catalyst support powders. Most importantly, this technique could easily be scaled up to industrial production.

2. Experimental

A schematic of the setup used for these experiments is shown in Fig. 1. A 2-inch-diameter (5.1 cm) magnetron sputter source was located 12 cm above a stainless-steel (SS) cup. The SS cup was tilted 45° from normal and was rotated at 43 revolutions/min with a stepper motor then was attached to the base of the SS cup. A second, smaller SS cup was placed inside the SS cup that was attached to the motor.

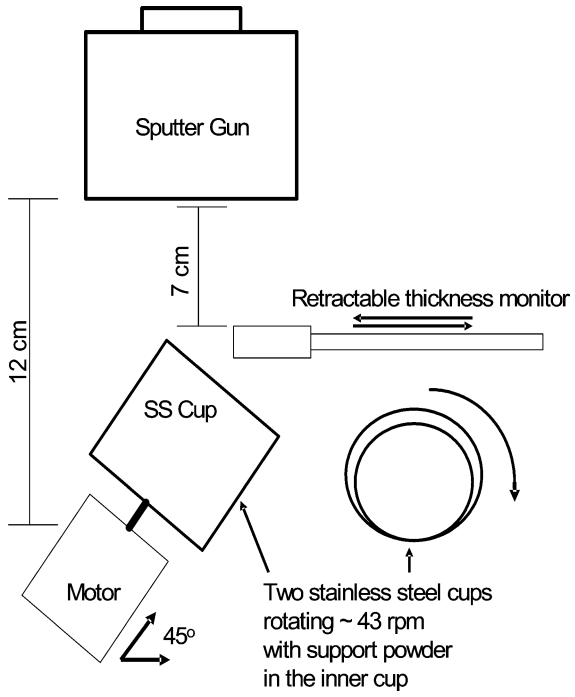

Fig. 1. Schematic representation of deposition chamber.

High-surface-area γ-Al_2O_3 (Baikalox-CR125, >99.99%, surface area $\sim 86\ m^2/g$) was dried at 250 °C for 6 h, then sieved through a 325-mesh sieve, and placed inside the smaller SS cup. The γ-Al_2O_3 (the major impurities were K, Na, and Si) was prepared by ammonium alum cracking. A gate valve was used to reduce the rate of air egress from the deposition chamber during the initial pump-down. If the chamber were evacuated too quickly, some of the support material would fly out of the SS cup and float to the bottom of the chamber. The chamber was evacuated until an initial vacuum of 3.0×10^{-6} torr or better was obtained. The SS cups were then rotated, causing the powders to tumble. A SS screw placed between the two SS cups caused the powders to be agitated when the smaller cup bumped over the screw, resulting in a constantly changing substrate orientation. The gold nanoparticles were prepared via direct current (dc) magnetron sputtering of a gold target (Englehard; 99.9%) in a high-purity Ar (Research Grade, 99.9995%; Air Liquide) atmosphere. The gold target was sputtered at an applied power of 11 W. The Ar was introduced into the chamber at a rate of 10 standard cubic centimeters per minute (sccm). The flow was adjusted to fix the total pressure of the system at 15 mtorr. The approximate deposition rate was determined with a Maxtek quartz crystal microbalance system positioned 7 cm above the tumbling powders. The measured rate of deposition at this height was 7.6 Å/s. At the end of the deposition process some of the support material was stuck to the side of the SS cup, but most of the powder was freely tumbling. To collect the powder, the SS cup was simply inverted on a piece of weighing paper. The powder that stuck to the side remained in the cup and was not used for subsequent work. The sample used in the rest of this study was prepared after 195 min of sputtering and is described here with the phrase "as-deposited."

The gold loading for the as-deposited material was determined with a Thermo Jarrell Ash IRIS inductively coupled plasma (ICP) optical emission spectrometer. Five mL of aqua regia (3:1 mixture of hydrochloric acid and nitric acid) was used to dissolve the Au from the samples for analysis. After reacting with the aqua regia, the samples were centrifuged and the γ-Al_2O_3 was separated from the acid and then washed three times with 18.3 MΩ deionized water. A series of ICP standards was prepared by serial dilution of an ICP standard prepared by Alfa-Aesar.

Catalytic activity of the as-deposited Au/Al_2O_3 powders toward the oxidation of CO was determined with a home-made catalyst test system. Approximately 0.04 g of the as-deposited catalytic powder was supported on a quartz frit sealed in a quartz tube. A series of mass flow control valves were used to send 50 sccm of gas through the powder bed (8 or 1 sccm CO, 4 sccm O_2, balance He). A vacuum system was attached downstream of the reactor tube, and a small amount of the product stream was sampled through a needle valve, which delivered it into the vacuum chamber. A resid-

ual gas analyzer (Vacscan Plus quadrapole mass spectrometer; Spectra Instruments) capable of detecting species with masses up to 100 amu was used to determine the product yield and conversion efficiency. All data were normalized to sample mass. To get a measure of the heat generated by the exothermic reaction, a K-type thermocouple was placed in direct contact with the outside of the quartz tube at the reactor bed.

A small quantity of the as-deposited material was furnace annealed under flowing argon at 400 °C for 2 h. This allowed us to compare three different samples of the catalytic powder, "as-deposited," "as reacted" with CO and O_2, and "annealed." We used a combination of X-ray photoelectron spectroscopy (XPS), scanning transmission electron microscopy (STEM), and powder X-ray diffraction (PXD) to investigate these materials.

A VG Microscopes HB603 UHV STEM operating at 300 kV equipped with an aberration corrector from the Nion Co. was used to image the Au samples. This system has been shown to have a resolution of better than 0.6 Å [20], although the main reason for using it was the sensitivity available in the high-angle annular dark-field imaging mode (HAADF). This provides Z-contrast imaging [21,22], where the brightness depends on the thickness and approximately the square of the atomic number. This mode is particularly suitable for investigating catalyst samples because even the smallest nanoparticles, including single gold atoms, are visible on real supports that can be up to several nanometers thick.

Powder X-ray diffraction data were collected on the powders with a Scintag X1 diffractometer with Cu-K_α radiation. Samples were mounted on a zero background sample holder. Data were collected from 10–90° 2θ over 2 h. X-ray photoelectron spectroscopy data were collected with a Perkin–Elmer 15 255G double-pass CMA attached to a standard UHV chamber. An Mg anode was used as a source and operated at 15 kV and an applied power of 400 W. XPS samples were mounted on a piece of carbon tape (Nisshin E.M. Co. Ltd). A piece of Au foil was used as a gold standard in order to calibrate the Au $4f_{7/2}$ binding energy (84.1 eV). The gold foil was sputtered with argon before use to ensure a clean surface. Binding energy shifts of the sample were referenced to a C 1s binding energy value of 284.5 eV [23].

3. Results and discussion

The as-deposited sample was a light purple color (Fig. 2). When the samples were annealed, their color remained purple. The total gold loading on the Al_2O_3 as measured by ICP was 1.37 wt%. Powder X-ray diffraction of the Al_2O_3 powder before deposition revealed that it was a mixture of α- and γ-Al_2O_3, although the exact ratio could not be determined because of the broad diffraction peaks of the γ-phase. There were no gold X-ray diffraction peaks observed for the as-deposited sample or any of the treated samples, either reacted or annealed. This is probably due to a combination of factors, including the small particle size, small grain size, and the relatively low concentrations of Au relative to the Al_2O_3.

Fig. 2. Picture of the as-deposited 1.37% Au/Al_2O_3 sample.

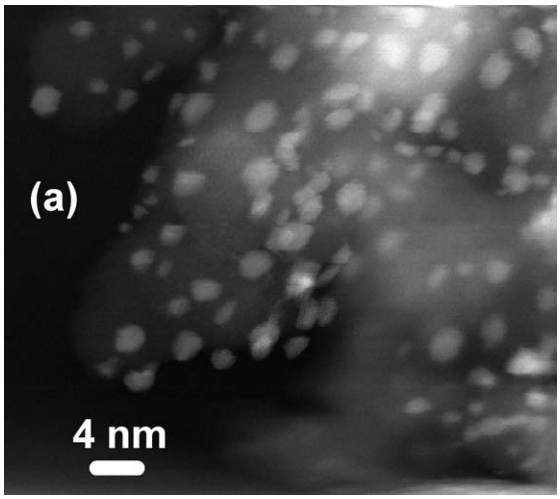

Fig. 3. Representative image of the as-deposited Au/Al_2O_3 sample.

STEM data for the as-deposited samples revealed that the gold particles were regular in size and shape and they were homogeneously distributed across the surface. A representative image of the gold nanoparticles on the surface of the Al_2O_3 is shown in Fig. 3. Fig. 4 (top) shows a histogram of the largest dimension measured for the gold particles. Particle sizes were determined with data from at least five images collected for different grains of Al_2O_3 in the STEM. At least 84 data points were collected for each sample to generate the histogram. We calculated the diameter of the nanoparticles by measuring the widest point of the nanoparticle. The gold particles have a mean width of about 2.3 nm, and 85% of the particles having a diameter less than 3 nm. We can estimate from the brightness of the gold nanoparticles and the apparent shape in Fig. 5 that most of the nanoparticles are thicker than two monolayers of gold. Closer inspection of the as-deposited gold particles reveals that they are approximately

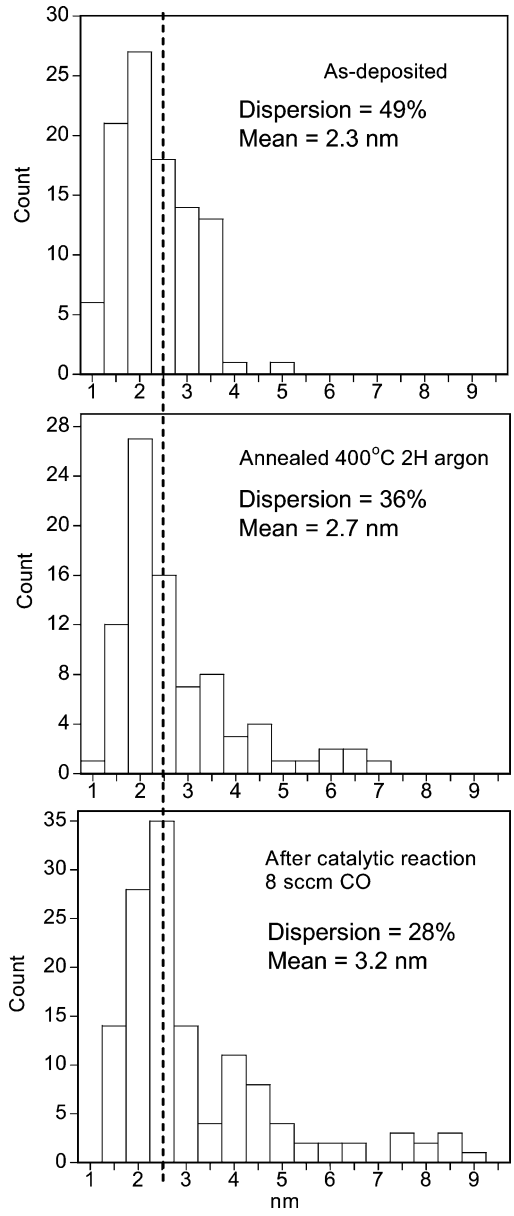

Fig. 4. (Top) Histogram of the maximum widths of the as-deposited nanoparticles. (Middle) Histogram of the maximum widths of the gold nanoparticles after annealing at 400 °C for 2H in flowing argon. (Bottom) Histogram of gold particle sizes after catalytic reaction with 8 sccm of CO.

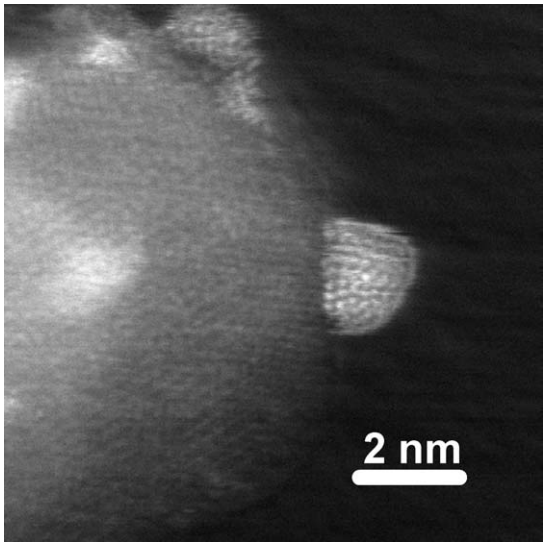

Fig. 5. View of a hemispherical gold particle on a as-deposited sample.

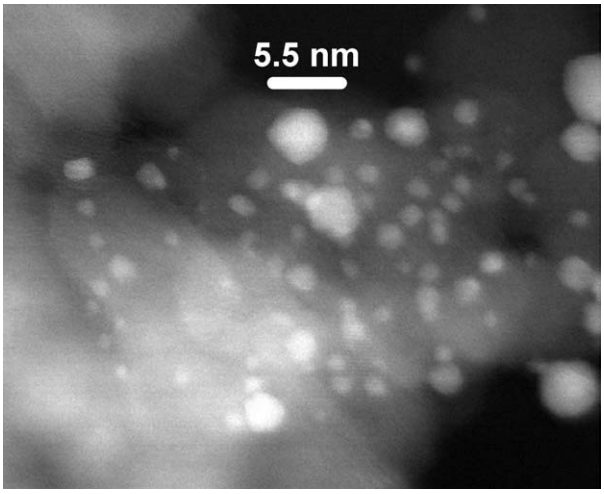

Fig. 6. Representative image of the Au/Al_2O_3 sample after annealing for 2H at 400 °C in flowing argon.

hemispherical (Fig. 5) and homogeneously distributed at the exposed surface. However, the particle coverage in the image is much higher than would be expected if the gold particles coated the total alumina surface uniformly. From BET surface area, Au loading, and average particle sizes, a uniform Au distribution would cover 1% of the surface. The surface coverage imaged in the STEM is clearly greater than 1%. By sputter coating, it is unlikely that gold atoms would be able to penetrate to the inner surfaces of agglomerates, or into deep pores. Hence most of the gold would be deposited on the outer surface of the alumina. Unfortunately, this cannot be verified by STEM images, as the larger agglomerates and particles are too thick to allow transmission of the electrons.

In order to estimate the thermal stability of the nanoparticles, a small portion of the as-deposited sample was annealed in flowing Ar for 2 h at 400 °C. Figs. 6 and 7 show images of this annealed sample, revealing clear agglomeration of some of the gold particles. However, even after annealing, the largest gold particles were only 6 nm in diameter, and the majority (75%) of the nanoparticles were still less than 3 nm in diameter. Fig. 7 shows a magnified image of one of the larger nanoparticles that formed during annealing. The gold nanoparticles became more symmetrical, and some formed hexagonal structures (Fig. 7). The planes shown in Fig. 7 correspond to the Au ⟨111⟩ lattice planes. Despite the high-temperature annealing, there still seems to be disorder within the nanoparticles, leading to multiple twinning, which is not unexpected, considering this is the stable form of gold nanoparticles [24,25].

Catalytic tests were performed with the use of a small portion of the as-deposited sample. For each catalytic test

Table 1
Comparison of Au on Al_2O_3 reactivity data

Method[a]	Au (wt%)	Mean diameter (nm)	Gas mixture	T (K)	Time (min)	Convert (%)	TOF	Ref.
CVD	5.3	3.5	1% CO/Air	273			0.01	[1]
DP	0.94	2.4	1% CO/Air	273			0.02	[11]
Co-PPT	4.2	3.5	1% CO/Air	273			0.006	[11]
DP	1.32	7.2	1% CO/Air	273	60	∼0		[38]
Mod. DP	1.73	3.4	1% CO/Air	273	60	∼0		[38]
CVD	4.58	4.1	1% CO/Air	273	60	∼100		[38]
IMP	0.43	n.d.	1% CO/0.5% O_2/N_2	297	60	57		[39]
IMP	0.43	n.d.	1% CO/Air	297	60	97		[39]
DP	1.1	3–5	1% CO/2.5% O_2/N_2	295	30	10	0.17–0.46	[40]
IMP	1	2.2	20% CO/10% O_2/He	298	60	12	0.49	[41]
MS	1.37	3.2	8% CO/4% O_2/He	300	120	17	1.1	This work
MS	1.37	3.2	1% CO/4% O_2/He	300	120	40	0.34	This work

[a] CVD = Chemical Vapor Deposition; DP = Deposition Precipitation; Mod. DP = Modified Deposition Precipitation; IMP = Impregnation; MS = Magnetron Sputtering; n.d. = not detectable.

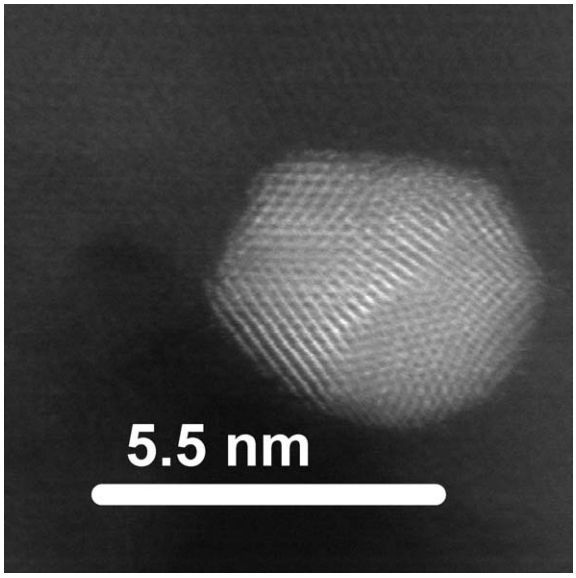

Fig. 7. View of a gold nanoparticle after annealing for 2H at 400 °C in flowing argon. The planes evident in the image correspond to the Au ⟨111⟩ planes. Notice the polycrystalline nature of the annealed particles.

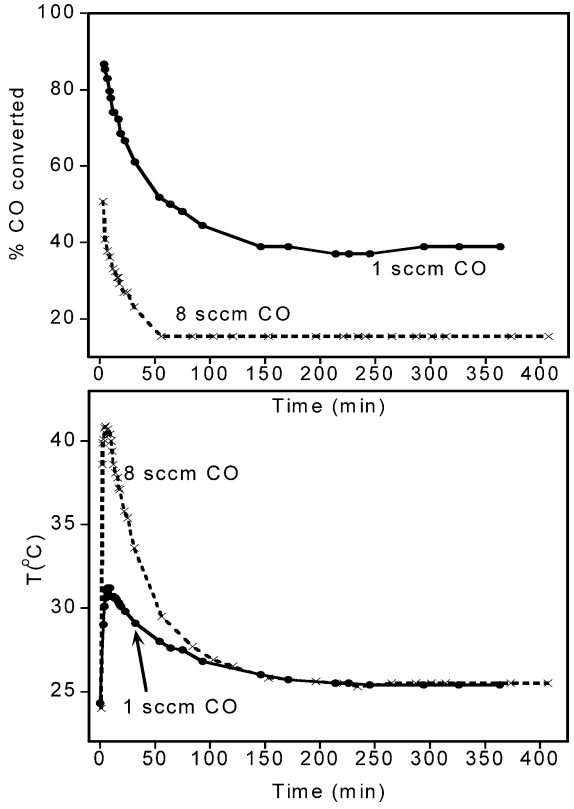

Fig. 8. (Top) Catalytic conversion of CO to CO_2 as a function of time for the as-deposited gold catalysts at 8 and 1 sccm of flowing CO (4 sccm O_2, balance He). (Bottom) Temperature measured outside of the reactor during the catalytic oxidation of CO.

a new portion of the as-deposited sample was used without the application of any pretreatments. Fig. 8 shows the room-temperature conversion efficiency versus time dependence of the as-deposited sample for the oxidation of carbon monoxide at two different CO flows, 1 sccm CO and 8 sccm CO. The bottom plot of Fig. 8 shows the temperature outside of the quartz tube (next to the reactor bed) as a function of time. Initially the conversion efficiency was very high, 87% (1 sccm CO) and 50% (8 sccm CO); however, there was a rapid decrease in activity as a function of time. After a period of time, the catalytic activity stabilized and remained constant for the remainder of the test. These steady conversion values correspond to an approximate turnover frequency (TOF) of 1.1 conversions/surface Au atom/s based on a 28% Au dispersion and 8 sccm of CO. For 1 sccm of CO the TOF after several hours is 0.34 conversions/surface Au atom/s. Table 1 compares the reported catalytic activity of other Au/Al_2O_3 catalysts and those prepared for this paper. The catalysts prepared by magnetron sputtering exhibit TOFs and steady-state activities similar to those of the other Au/Al_2O_3 samples; however, direct comparisons are difficult because of different reaction conditions. The amounts of CO and O_2 that were consumed and the amount of CO_2 produced were stoichiometric. The temperature measured out-

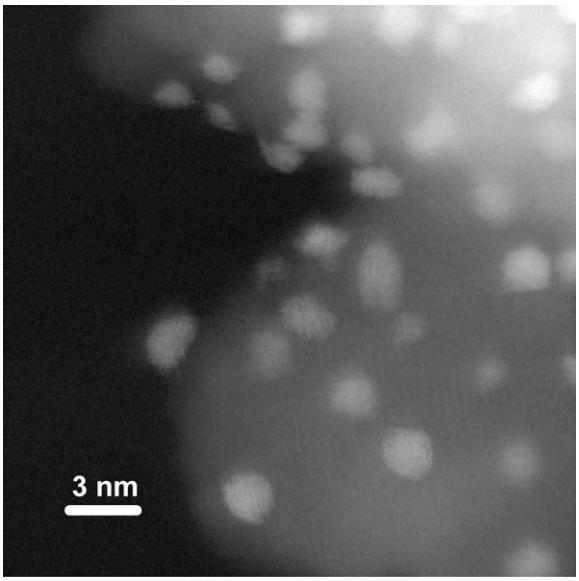

Fig. 9. STEM image of Au after 8 sccm CO oxidation reaction.

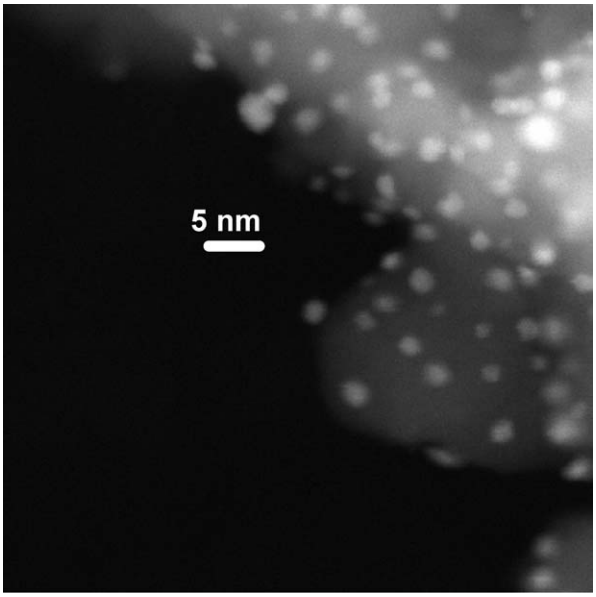

Fig. 10. Image of the catalyst surface used for the 8 sccm CO oxidation reaction.

side of the catalytic reactor followed the same profile as the conversion efficiency plot. The temperature increased only when all three gases were flowing through the bed. When CO or O_2 was absent, no increase in temperature was observed, so heating was clearly due to the exothermic oxidation reaction ($\Delta G = -257\ \mathrm{kJ/mol_{CO_2}}$). Deactivation of gold catalysts has been reported before and has been attributed to a variety of factors, including gold agglomeration and carbon-containing impurities [3]. To determine the effect of in-situ reaction heating of the catalysts, STEM images were collected on a sample that was used for the 8 sccm CO oxidation reaction.

Fig. 4 (bottom) shows a histogram of the gold particle sizes after the 8 sccm CO oxidation reaction. STEM

Table 2
Binding energies of the as-deposited and 8 sccm CO reacted samples

Element	Binding energy (eV)	
	As-deposited	After catalytic reaction
Al 2p	74.4	73.7
Al 2s	119.5	118.7
C 1s[a]	284.5	284.5
O 2s	23.5	23.5
O 1s	531.0	531.0
Au $4f_{7/2}$	83.7	83.0
Au $4f_{5/2}$	87.3	86.3
Au 5s	110.8	110.7
Au $4d_{5/2}$	334.5	334.1
Au $4d_{3/2}$	353.5	352.3

[a] Charging effects corrected for by fixing the C 1s binding energy to 284.5 eV.

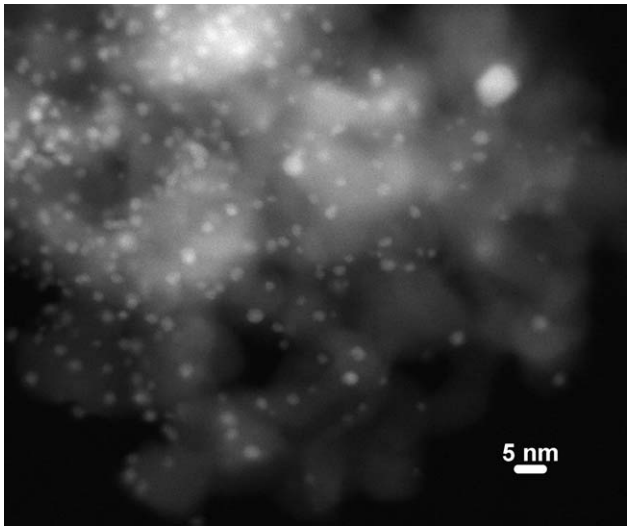

Fig. 11. Image of the catalyst surface used for the 8 sccm CO oxidation reaction.

data show that the particles appeared to be symmetrical (see Figs. 9–11). After 7 h of reaction, 80% of the particles were still less than 4 nm across. However, several larger particles of gold (> 6 nm) were visible. The large gold particles were bigger than those that formed during the 2-h annealing experiment. Despite the larger gold particles, the sample remains catalytically active (Fig. 8).

To glean more information about the gold nanoparticles, XPS studies were performed on the as-deposited and 8 sccm CO reacted samples. XPS data for the as-deposited gold sample (Fig. 12 and Table 2) revealed that the Au $4f_{7/2}$ binding energy is shifted by −0.4 eV to 83.7 eV relative to the binding energy of the gold standard (84.1 eV). The Al 2p and 2s and the O 1s binding energies all correspond to the binding energies reported in the literature [23]. The XPS data also reveal that there are no impurities on the surface of our samples [e.g., Cl (Fig. 3)]; however, carbonaceous species on the surface could not be accurately observed because the

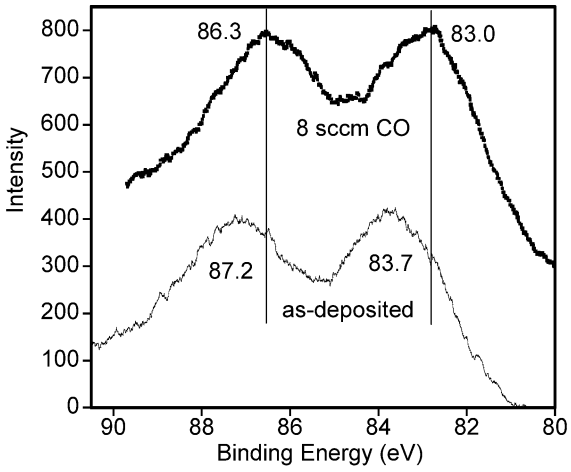

Fig. 12. Au-XPS data for the as-deposited Au/Al_2O_3 sample (bottom) and sample that was used in the 8 sccm CO oxidation reaction.

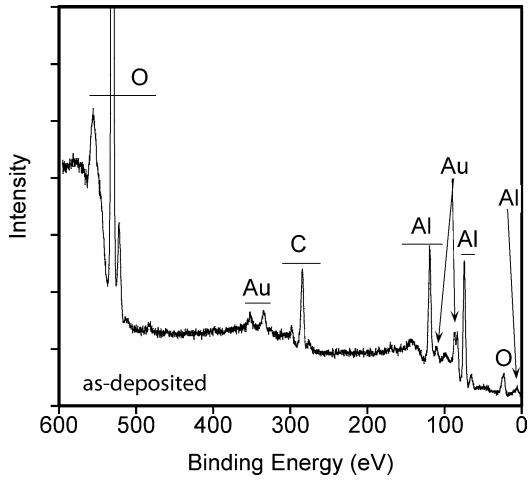

Fig. 13. XPS survey scan of the as-deposited sample.

samples were mounted on carbon tape. The XPS data collected for the reacted sample revealed significant shifts to still lower binding energies of the Au $4f_{7/2}$ peak (83.0 eV, shift of −0.7 eV, Fig. 12, top, and Table 1) or a shift of −1.1 eV relative to the gold standard. The Al 2p and 2s binding energy also shifted by −0.7 eV (Fig. 14 and Table 2), whereas the O 1s binding energy remained unchanged. None of the gold XPS data show any indication of Au^{3+} or Au^{1+} (BE Au^{3+} $4f_{7/2} = 85.5$; Au^{1+} $4f_{7/2} = 84.5$ eV) [23] cations present in the samples. At this point, without Mössbauer data, it is impossible to conclusively determine whether all of the Au is metallic or anionic.

The shift to lower binding energy has been reported for gold clusters or nanoparticles on Al_2O_3 and is attributed to several effects. Some investigators attribute the shift to electron transfer from the alumina to the metallic gold due to the larger electronegativity of gold relative to Al^{3+} [13,26,27]. Similar effects are observed for Au on TiO_2 and ZrO_2 [28,29]. However, recent work by Radnik et al. indicates that particle shapes could be a critical factor in determining the negative BE shifts of gold-supported nanoparticles [30]. Radnik et al. indicate that the more spherical the nanoparticles, the lower the binding energy (down to 83.0 eV for Au on TiO_2) [30]. This shift is due to initial state effects where spherical particles have less coordinated surface atoms, which reduces their binding energies relative to nanoparticles with large faces [30,31]. For the current study, when only ∼ 28% of the gold atoms are exposed, the shape of the particle has a smaller effect on the negative binding energy shifts. The origin of the shift is therefore probably due to enhanced charge transfer from the substrate to the nanoparticles after the reaction. This transfer may be correlated with the observed shift in Al binding energies.

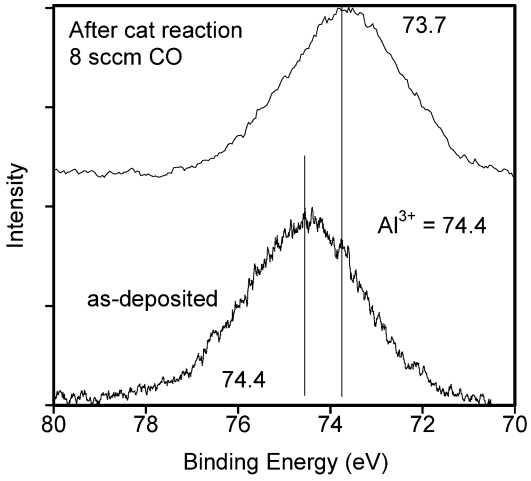

Fig. 14. Al 2p XPS data for the as deposited Au on Al_2O_3 sample (bottom) and following the 8 sccm CO oxidation reaction.

Despite the large shift (−0.7 eV), the Al 2p binding energy still corresponds to an Al^{3+} ion [23,32,33]. The origin of this shift might be attributed to increased interactions between the Au and Al_2O_3 [34]; however, the shift could also be due to subtle structural changes in the Al_2O_3 at the surface, such as the $\gamma \rightarrow \delta \rightarrow \theta$ Al_2O_3 phase transition, resulting in a slightly modified Al^{3+} binding energy [35,36]. The large amount of energy released during the CO oxidation reaction could be enough to promote local surface changes after several hours on stream [35]. Another possibility could be the formation of a Au–Al alloy [37]. However, this seems unlikely, since the STEM shows no indication of alloy formation. In addition, the majority of the Al XPS signal would still be from the Al_2O_3, and it would be expected that a shoulder or a broader peak would occur for the Al.

4. Conclusion

Gold nanoparticles with average diameters between 2 and 3 nm were deposited on γ-Al_2O_3 via dc sputtering of a gold target. Microscopy results show that the as-deposited gold is hemispherical. Reactivity of these particles was demonstrated by the oxidation of CO. The results show that the nanoparticles are active catalysts at room temperature and can convert up to 40% of the CO after 6 h on stream. STEM

data show that after catalysis of the oxidation of CO for 7 h or, alternatively, heating of the sample at 400 °C for 2 h, larger gold particles (up to 9 nm in diameter) are formed. However, 64% of the gold nanoparticles still have diameters between 2 and 3 nm.

The technique used to prepare the nanoparticles has several advantages that make it attractive for industrial applications, such as no waste stream, cheap reagents, and scalability. In addition, this preparation method can be applied to almost any substrate, is stable in vacuum, and can use almost any metal particles. We have applied this technique the preparation of Pt, Cu, and Mn nanoparticles on Al_2O_3, and Au on carbon. These results will be reported in subsequent publications.

Acknowledgments

The authors thank Tamara Keever of ORNL's Chemical Sciences Division for assistance with ICP and Art Baddorf for help with XPS. This research was sponsored by the U.S. Department of Energy's Division of Materials Science under contract DE-AC05-00OR22725, with ORNL, managed and operated by UT-Battelle, LLC. G.M.V. and A.R.L. were supported by appointments to the Oak Ridge National Laboratory Postdoctoral Research Associates Program, administered jointly by the Oak Ridge Institute for Science and Education and Oak Ridge National Laboratory.

References

[1] M. Haruta, N. Yamada, H. Kobayashi, S. Iijima, J. Catal. 115 (1989) 301.
[2] A. Wolf, F. Schüth, Appl. Catal. A: Gen. 226 (2002) 1.
[3] G.C. Bond, D.T. Thompson, Catal. Rev.-Sci. Eng. 41 (1999) 319.
[4] G.C. Bond, Catal. Today 72 (2002) 5.
[5] M. Haruta, The Chem. Record 3 (2003) 75.
[6] M. Haruta, Catal. Today 36 (1997) 153.
[7] M. Haruta, Gold Bull. 37 (2004) 27.
[8] G. Schmid, B. Corain, Eur. J. Inorg. Chem. 2003 (2003) 3081.
[9] L. Zhang, F. Cosandey, R. Persaud, T.E. Madey, Surf. Sci. 439 (1999) 73.
[10] M. Valden, X. Lai, D.W. Goodman, Science 281 (1998) 1647.
[11] M. Okumura, S. Nakamura, S. Tsubota, T. Nakamura, M. Azuma, M. Haruta, Catal. Lett. 51 (1998) 53.
[12] M. Okumura, K. Tanaka, A. Ueda, M. Haruta, Solid State Ionics 95 (1997) 143.
[13] S. Arrii, F. Morfin, A.J. Renouprez, J.L. Rousset, J. Am. Chem. Soc. 126 (2004) 1199.
[14] J.A. Cairns, R.S. Nelson, R.W. Barnfield, UK 1537839 (1979).
[15] A. Takeuchi, H. Wise, J. Catal. 83 (1983) 477.
[16] P. Albers, K. Seibold, A.J. McEvoy, J. Kiwi, J. Phys. Chem. 93 (1989) 1510.
[17] B. Wang, Z. Ji, F.T. Zimone, G.M. Janowski, J.M. Rigsbee, Surf. Coat. Technol. 91 (1997) 64.
[18] W. Ensinger, H.R. Müller, Surf. Coat. Technol. 163–164 (2003) 281.
[19] T. Kobayashi, M. Haruta, S. Tsubota, H. Sano, B. Delmon, Sensors and Actuators B 1 (1990) 222.
[20] P.D. Nellist, M.F. Chisholm, N. Dellby, O.L. Krivanek, M.F. Murfitt, Z.S. Szilagyi, A.R. Lupini, A. Borisevich, W.H. Sides Jr., S.J. Pennycook, Science 305 (2004) 1741.
[21] S.J. Pennycook, P.D. Nellist, in: D.G. Rickerby, U. Valdré, G. Valdré (Eds.), Impact of Electron and Scanning Probe Microscopy on Materials Research, Kluwer-Academic, Dordrecht, 1999, p. 166.
[22] P.D. Nellist, S.J. Pennycook, Adv. Img. Elect. Phys. 113 (2000) 147.
[23] J.F. Moulder, W.F. Stickle, P.E. Sobol, K.D. Bomben, Handbook of X-ray Photoelectron Spectroscopy, Perkin–Elmer Corp., Eden Prairie, MN, 1992.
[24] L.D. Marks, D.J. Smith, J. Crystal Growth 54 (1981) 425.
[25] D.J. Smith, L.D. Marks, J. Crystal Growth 54 (1981) 433.
[26] S. Shukla, S. Seal, NanoStruct. Mater. 11 (1999) 1181.
[27] M.G. Mason, Phys. Rev. B 27 (1983) 748.
[28] A. Zwijnenburg, A. Goossens, W.G. Sloof, M.W.J. Crajé, A.M. van der Kraan, L.J. de Jongh, M. Makkee, J.A. Moulijn, J. Phys. Chem. B 106 (2002) 9853.
[29] S. Zafeiratos, S. Kennou, Surf. Sci. 443 (1999) 238.
[30] J. Radnik, C. Mohr, P. Claus, Phys. Chem. Chem. Phys. 5 (2003) 172.
[31] C.R. Henry, Surf. Sci. Rep. 31 (1998) 231.
[32] C.D. Wagner, D.E. Passoja, H.F. Hillery, T.G. Kinisky, H.A. Six, W.T. Jansen, J.A. Taylor, J. Vac. Sci. Technol. 21 (1982) 933.
[33] J.A. Taylor, J. Vac. Sci. Technol. 20 (1982) 751.
[34] T. Ishizaka, S. Muto, Y. Kurokawa, Opt. Commun. 190 (2001) 385.
[35] S.J. Wilson, J.D.C. McConnell, J. Solid State Chem. 34 (1980) 315.
[36] O. Böse, E. Kemnitz, A. Lippitz, W.E.S. Unger, Fresenius J. Anal. Chem. 358 (1997) 175.
[37] H. Piao, N.S. McIntyre, Surf. Interface Anal. 31 (2001) 874.
[38] Y.-J. Chen, C. Yeh, J. Catal. 200 (2001) 59.
[39] S.-J. Lee, A. Gavriilidis, J. Catal. 206 (2002) 305.
[40] C.K. Costello, M.C. Kung, H.-S. Oh, Y. Wang, H.H. Kung, Appl. Catal. A: Gen. 232 (2002) 159.
[41] Q. Xu, K.C.C. Kharas, A.K. Datye, Catal. Lett. 85 (2003) 229.